J. Fluid Mech. (1997), *vol.* 338, *pp.* 231–248

Printed in the United Kingdom © 1997 Cambridge University Press

Global dynamics and aerodynamic flow vectoring of wakes

By D. A. HAMMOND AND L. G. REDEKOPP

Department of Aerospace Engineering, University of Southern California, Los Angeles, CA 90089–1191, USA

(Received 25 October 1995 and in revised form 9 August 1996)

A methodology for vectoring the near-wake flow behind a bluff body without any mechanical movement of the physical boundaries of the generating body is described. The sole control input is suction applied at the fixed base of the forebody. Once the suction volume flux exceeds a critical value needed to suppress the global dynamics associated with vortex shedding, local directional control of the near wake can be achieved. The distribution of suction velocities across the base can be varied to obtain proportional directional control. The role of symmetries in stimulating aerodynamic vectoring of a streaming flow is emphasized and illustrated.

1. Introduction

Mechanical flow control devices such as flaps, elevators, etc. are used extensively on aerodynamic surfaces to achieve lift augmentation and attitude control. This class of movable control devices has recently been incorporated at jet exhausts to accomplish thrust vectoring control for rapid, or enhanced, vehicle manoeuverability, including post-stall performance (cf. Ashley 1995). Even though their application in recent years has led to the realization of quite spectacular manoeuvers, the technology often involves a significant weight penalty, because of the actuator hardware, and a low fatigue life because of severe unsteady loading and direct exposure of control surfaces to high-temperature streams. Another limitation is the slow response time arising from inertia inherent in mechanical systems. For these reasons, and others, it is of some interest to identify *aerodynamic* means of vectoring a flow; that is, to identify methodologies where an external or ducted flow can be re-directed entirely by alteration of boundary conditions and without any mechanical movement of surfaces which guide or constrain the flow. The present work describes a strategy for the aerodynamic flow vectoring of the near wake behind a blunt-based forebody. The aerodynamic control is achieved through suction applied in the base region where the two streams on opposite sides of the planar-shaped forebody separate and form the wake.

Several approaches to vectoring of jets by aerodynamic or fluidic means have been proposed and studied. Fluidic logic devices and jet amplifiers use secondary injection to stimulate directional switching, but the response is usually bistable and not proportional. Some devices also employ Coanda attachment of the primary flow in conjunction with secondary transverse jets (cf. Gilbert 1993). A promising alternative approach has recently been proposed and tested by Washington *et al.* (1996). A low-aspect-ratio two-dimensional jet was designed with a contoured 'collar' on each side which extends beyond the jet exit. Suction is applied on either side

https://doi.org/10.1017/S0022112096004818 Published online by Cambridge University Press

of the jet through the gap between the collar and the divergent section of the jet boundary. A counter-current mixing layer is created on the suction side of the jet with the dynamic effect of a pronounced increase in the local entrainment rate when the suction mass flux exceeds a critical value. The response of the jet is to veer toward the collar on the suction side. Significant vectoring angles have been realized (up to 16°) with minimal loss of thrust. A different scheme involving the use of piezoelectric actuators placed along a blunt face of the exit of a two-dimensional jet has been demonstrated by Smith & Glezer (1994). When an actuator on either side is operating, a zero-mass-flux jet is created which interacts with the primary jet in such a way as to 'attract' the primary jet toward the actuator-induced jet. The transverse force responsible for vectoring the primary jet may arise from the formation of a local separation inside the jet near the exit, but the underlying mechanism for vectoring is not completely clear.

The vectoring of a streaming flow, a flow in which the streamlines of the time-averaged state are nearly parallel, implies that the symmetry of the flow is altered by the application, or by the inducement, of a localized force. In mechanical means of flow vectoring this is accomplished through actuators which change the position of control surfaces, thereby constraining the adjacent flow to move along an altered path. In aerodynamic flow vectoring the flow re-direction is achieved through enforcement of altered boundary conditions. Aerodynamic flow vectoring is closely linked to the symmetry properties of the streaming flow and the boundary conditions. If there is any asymmetry in the pre-existing streaming flow, this can be exploited through modified boundary conditions, which may even be applied symmetrically, to induce a symmetry-breaking of the mean flow streamline pattern. On the other hand, if the original flow has a high level of symmetry, asymmetrically applied boundary conditions are required to stimulate a resulting asymmetric flow pattern. Hence, the underlying symmetry of the flow which is to be vectored is an important consideration in designing a strategy for the aerodynamic vectoring of a flow and in defining its potential for vectoring (i.e. the vectoring response in comparison to the control power required to achieve the vectored state). These issues will become apparent in the results which follow.

The vectoring response of a streaming flow also depends on the nature of local instabilities and the existence, or lack thereof, of any global instabilities. Distinctions between local and global instability, and the character of local instabilities, are quite important to the issues of flow control in general and to the problem of flow vectoring in particular. A discussion of these issues and their relation to the receptivity of a flow to localized forcing is presented by Ho & Huerre (1984) and by Huerre & Monkewitz (1990). It is now firmly established that flows whose local instability is of convective type throughout its streamwise development are quite receptive to upstream disturbances. Small upstream disturbances which exploit the natural amplifier of the unstable system can significantly alter the downstream evolution of the flow. This receptivity of the flow to injected disturbances is lost when the flow is locally absolutely unstable. In this case the control input required to achieve significant flow modification is a significant fraction of the energy of the basic flow. Another possible flow scenario is one where the local instability is of mixed type, yet globally stable. An example of such a state is the spatially developing flow behind a two-dimensional bluff body when the Reynolds number is below the critical value for the onset of vortex shedding. At sufficiently low Reynolds numbers, local profiles of the wake are unstable on a quasi-parallel basis but the flow remains steady because of global stability. However, when the Reynolds number exceeds the

https://doi.org/10.1017/S0022112096004818 Published online by Cambridge University Press

critical value and the region of local absolute instability grows to sufficient size, a Hopf bifurcation occurs giving birth to a globally unstable state (on a linear basis) which is subsequently saturated through nonlinear effects (cf. Mathis, Provansal & Boyer 1984; Sreenivasan, Strykowski & Ollinger 1986; Provansal, Mathis & Boyer 1987; and Schumm, Berger & Monkewitz 1994). The resulting vortex-shedding state is definable in terms of a global mode which characterizes the flow over its global extent. The onset of global instability endows the spatially developing flow with a certain 'rigidity' in that efforts to vector the flow by control actions requires a manipulation (or vectoring) of the whole streamwise eigenfunction underlying the global instability. Obviously, the vectoring potential for such flows is very low. If, on the other hand, the global instability can be suppressed through some control action, then the potential for local vectoring of the separating, near-wake flow is expected to increase dramatically. Results presented subsequently are directed toward the validation of this approach in vectoring the near-wake flow behind a bluff body. Preliminary experimental validation of the methodology described here is provided by Leu & Ho (1993), which originated as a companion part of the present study.

The terms global instability, global mode, and vortex-shedding state are used interchangeably throughout the text which follows. The term global mode implies the existence of a streamwise eigenmode which defines the spatial organization in the streamwise direction of the velocity and vorticity fields. This mode has a discrete frequency which defines the temporal character of dynamical quantities at any spatial position in the wake. In this sense a global mode is a mathematical entity, but physical flow quantities are immediately describable in terms of the eigenfunction for the mode. The term global instability refers to the fact that this global mode is linearly unstable. However, the instability sets in via a supercritical Hopf bifurcation and, hence, is saturated by nonlinearity. It is true, however, that any observable equilibrium global mode is a nonlinear entity. The dynamics of an active global mode are manifested physically as a periodic vortex shedding from the bluff body creating the spatially developing wake flow.

The essential features in the approach to aerodynamic flow vectoring of a wake described here can be summarized in three steps. First, the presence of a region of local absolute instability in the spatially developing wake flow can, if the region of absolute instability exceeds a critical size, trigger a global instability. Second, if a global instability is present in a flow, the vectoring potential of that flow is greatly enhanced when control inputs are employed which suppress the global instability. The use of base suction as a means of flow control is effective in suppressing a global instability in a wake through modification of local instability characteristics. Next, one can use asymmetrically applied suction to induce local vectoring control of the globally stable near-wake flow. Suction accentuates asymmetry in the near-wake flow through asymmetrically induced entrainment from the boundary layers on either side of the forebody.

2. Problem definition

We study the planar flow formed by the passage of two parallel streams with independent ambient velocities over a forebody with a rectangular-shaped trailing edge of height b. We choose to make all variables dimensionless using the base height b as the reference length scale and the average velocity U_∞ of the two independent streams as the reference velocity scale. The flow on either side of the forebody consists of uniform ambient flows with (dimensionless) speeds U_1 and U_2 and Blasius

https://doi.org/10.1017/S0022112096004818 Published online by Cambridge University Press

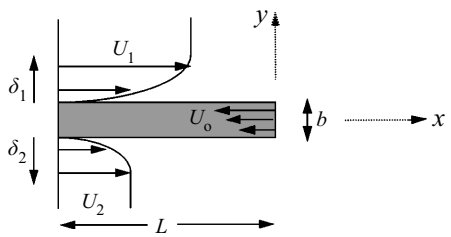


FIGURE 1. Schematic of the flow configuration.

boundary layers with (dimensionless) thickness δ_1 and δ_2, respectively, adjacent to the sides of the forebody. A wake-shear layer develops downstream of the forebody which can be characterized in terms of a Reynolds number R and a velocity ratio r defined as

$$R = \frac{U_\infty b}{\nu}, \quad r = \tfrac{1}{2}(U_1 - U_2), \tag{2.1}$$

where ν is the kinematic viscosity of the homogeneous incompressible fluid. The control variable for the flow is the (dimensionless) suction velocity $U_0(y)$ which is distributed across the base of the forebody. An alternative measure of the control is the suction volume flux (per unit span)

$$q = \int_{-1/2}^{1/2} U_0(y)\,\mathrm{d}y. \tag{2.2}$$

A schematic of the flow configuration is presented in figure 1. We suppose that the high-speed stream is always positioned on the upper side of the forebody as shown in this figure.

The flow described above is studied by direct numerical simulation. The QUICKEST (Quadratic Upwind Interpolation for Convective Kinetics with Estimated Streaming Terms) scheme originated by Leonard (1979) was employed for the solution of the unsteady equations of motion in two space dimensions. The no-slip boundary conditions were applied at the body surface with the exception of the normal velocity along the base which was prescribed by $U_0(y)$. The production version of the code was constructed with a two-level mesh wherein a uniform grid was used in the central strip reaching to the outer edges of each boundary layer and extending from the inlet to the exit of the domain. In the domains outside this strip, and extending to 20 units from the forebody surfaces where the streamwise velocity component was set equal to the ambient velocity, the grid in the transverse direction was stretched by a factor of 8% per interval. The inlet flow consisting of uniform streams with boundary layers at the forebody surfaces was prescribed at a position upstream of the base. At the downstream end of the computational domain, which was nominally positioned at 20 units downstream of the base, convective outflow boundary conditions were applied. Further details of the numerical approach and its validation are described in Hammond & Redekopp (1996).

The results presented herein are limited to low Reynolds numbers in the interest of performing simulations covering a reasonable range of the parameter space with limited computer resources. Furthermore, existing calculations for cylinder wakes show that three-dimensional effects appear for Reynolds numbers exceeding about $(4.3 \pm 0.1)R_{crit}$. The critical Reynolds number for the onset of vortex shedding for sheared wakes behind a rectangular-based forebody is shown in figure 2. Hence, the

https://doi.org/10.1017/S0022112096004818 Published online by Cambridge University Press

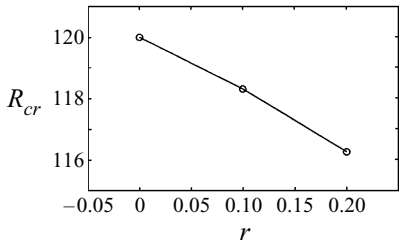


FIGURE 2. The critical Reynolds number for the onset of vortex shedding in the wake-shear layer behind a rectangular-based forebody with $\delta = 1.2$.

highest Reynolds number used in the simulations reported here is $R = 520$ and the grid spacing in the central strip of the computational domain was $\Delta x = \Delta y = 0.1$. This choice of grid also limits the range of inlet boundary layer thickness, an independent parameter in the present formulation, which can be realistically specified. Calculations are reported for boundary layer thicknesses in the range $0.6 < \delta_{1,2} < 1.2$, which translates into displacement thicknesses δ^* in the range $0.2 < \delta^*_{1,2} < 0.4$. Grid refinement studies suggest that the selected grid parameters yield results for global parameters such as the shedding frequency which are accurate to a few percent.

3. Relevant global dynamics

Before discussing simulations of the development of the sheared wake flow with base suction, some relevant results relating to the global dynamics of the flow in the absence of any applied control are reviewed. The definitive establishment of these results, together with a more amplified discussion and reference to related work, can be found in Hammond & Redekopp (1996).

The onset of vortex shedding (or, equivalently, the destabilization of the least-damped global mode) is intimately connected to the existence of a region of local absolute instability in the near-wake region of the spatially developing flow field (cf. Chomaz, Huerre & Redekopp 1988, 1991). In particular, the destabilization of the gravest global mode depends on some integral measure of the absolute growth rate over the region where it is positive. Furthermore, the existence of a locally absolutely unstable flow is related to the form of the velocity profile (principally, the wake deficit and, to some extent, the thickness of the two layers of vorticity comprising the wake profile). The latter result is perhaps most clearly demonstrated by Monkewitz (1988) where the character of the instability for a family of wake profiles is examined. Hence, any control input which modifies the shape of the velocity profiles, and thereby changes the distribution of local growth rates, can exert an influence on the global dynamics of the wake. In particular, suction can exert an influence in two competing ways. First, it will increase the velocity deficit at a fixed position in the near wake leading to enhanced absolute instabilities at that position. On the other hand, suction will tend to pull the saddle point of the time-averaged streamline pattern (i.e. the spatial extent of the near wake) closer to the base, thereby decreasing the streamwise extent of the region of local absolute instability. These two effects are illustrated in figure 3 where local absolute growth rates $\omega_{0_i}(x)$ (i.e. the temporal growth rate of a wavenumber having vanishing group velocity) and the position x_{AU} where $\omega_{0_i}(x_{AU}) = 0$ are plotted for different values of the uniformly

https://doi.org/10.1017/S0022112096004818 Published online by Cambridge University Press

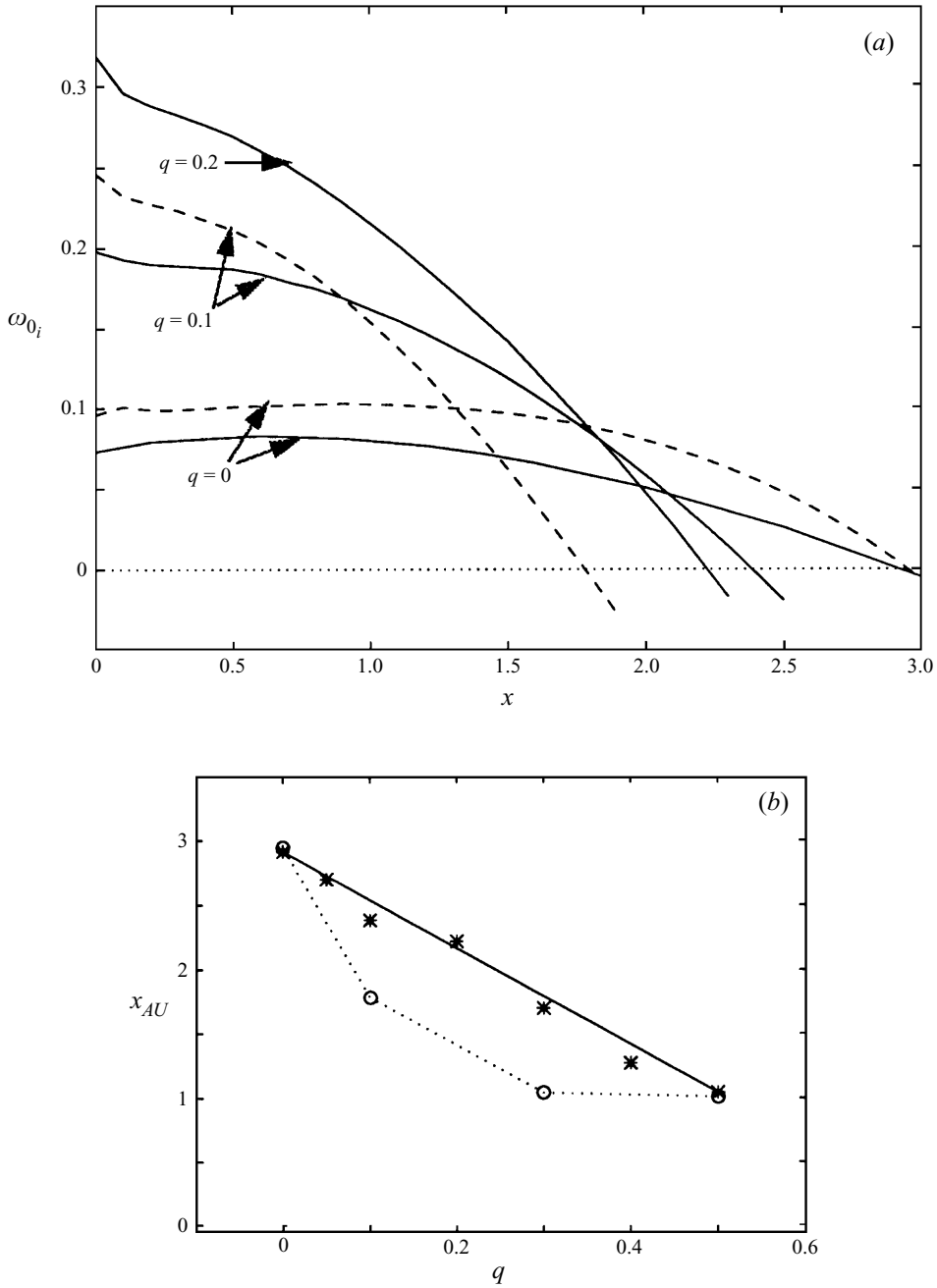


FIGURE 3. (*a*) The absolute growth rate and (*b*) streamwise length x_{AU} of the absolutely unstable region: —, $R = 160$; - - - (*a*), ····· (*b*), $R = 320$.

distributed suction velocity in a sheared wake with $r = 0.2$ at two different Reynolds numbers. The results were obtained from numerical simulations based on the same problem and algorithm described above plus the use of an Orr–Sommerfeld solver using computed local mean velocity profiles. The two effects of suction are evident in

https://doi.org/10.1017/S0022112096004818 Published online by Cambridge University Press

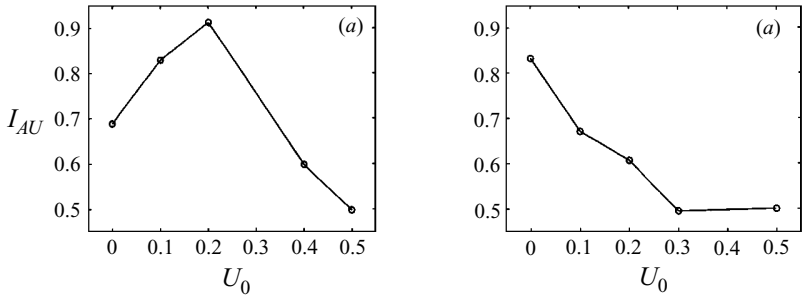


FIGURE 4. The variation of the integral parameter I_{AU} with suction velocity for the asymmetric wake with $r = 0.2$. (*a*) $R = 160$; (*b*) $R = 320$.

the figure and are clearly competing, at least insofar as the suppression of an active global mode is concerned.

Chomaz, Huerre & Redekopp (1990) conjectured that the quantity

$$I_{AU} = \int_0^{x_{AU}} (\omega_{0_i}(x))^{1/2} \mathrm{d}x \tag{3.1}$$

should exceed some critical value for the destabilization of the gravest global mode. No firm theoretical basis exists for the use of this quantity, but some global measure of $\omega_{0_i}(x)$ is believed to define the onset of global dynamics. The quantity defined in (3.1) is, at least, consistent with the model problems considered by Chomaz *et al.* (1988). Evaluation of I_{AU} for a wake with $r = 0.2$ at two Reynolds numbers is shown in figure 4 for cases where a uniform suction velocity is applied across the base. The boundary layer thicknesses in each case were fixed at $\delta_1 = \delta_2 = 1.2$. The sensitive evaluation of mean velocity profiles and values of ω_{0_i} very near the base, especially at higher suction velocities, introduces some uncertainty in computed values of I_{AU}, but the results shown in figure 4 are believed to be accurate to at least 0.025. The non-monotonic variation of I_{AU} observed in figure 4(*a*) arises from the competition described above between increasing values of ω_{0_i} near the base and decreasing values of x_{AU} as the suction flux is progressively enhanced. The increasing values of ω_{0_i} dominate the calculation of I_{AU} initially, but eventually the decreased value of x_{AU}, together with the square-root operation, yields declining values for I_{AU}. Although these computations show that suction applied at the base does not always produce a monotonic decline in I_{AU} as the volume flux is increased, they do suggest that suction may be effective in suppressing global dynamics in wake flows, at least insofar as I_{AU} is representative of the true global instability criterion.

Spurred by the foregoing results, a sequence of simulations was undertaken to identify the critical suction velocity required to suppress vortex shedding when the distribution of suction velocities was uniform across the base. Note that the value of U_0 in this case is equal to the suction volume flux normalized by the average velocity U_∞ and the base height b (cf. equation (2.2)). Results from this sequence of simulations for $\delta_1 = \delta_2 = 1.2$ are summarized in figure 5. For values of U_0 below the curves in each panel of the figure, vortex shedding is active. However, when U_0 exceeds a critical value, say $U_{0_{crit}}$, vortex shedding is always suppressed. It is observed that the value of $U_{0_{crit}}$ is tending to a plateau as the Reynolds number increases and that this critical value decreases quite rapidly, at fixed Reynolds numbers, as the mean flow asymmetry (i.e. shear) increases. These trends are encouraging relative

https://doi.org/10.1017/S0022112096004818 Published online by Cambridge University Press

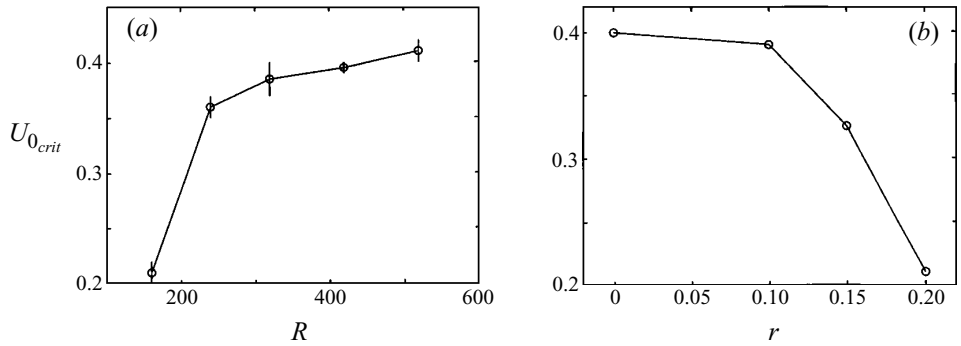


FIGURE 5. The critical suction velocity required to suppress vortex shedding in the wake-shear layer behind a rectangular-based forebody. (*a*) $r = 0.2$; (*b*) $R = 160$.

to scaling the present low-Reynolds-number results to parameter regimes realized in many applications.

We note at this juncture that the effect of the boundary layer thickness on the value of the critical suction velocity enters primarily through the Reynolds number. When global wake parameters such as the shedding frequency are considered, the effect of boundary layers on the forebody is captured by using a Reynolds number defined with a length scale equal to the sum of the base height plus the two displacement thicknesses evaluated at separation. Although we have conducted a range of simulations aimed at validating this effect in relation to $U_{0_{crit}}$ by varying $\delta_{1,2}$ by a factor of two, our results fall within the error band for obtaining $U_{0_{crit}}$. Precise evaluation of $U_{0_{crit}}$ is complicated by the vanishing of the growth rate of the global mode as U_0 approaches $U_{0_{crit}}$. Transients decay very slowly as the growth rate of the global instability tends toward zero and long integration times are required to accurately define the dynamics.

4. Flow vectoring results

It was observed in the course of carrying out the sequence of simulations summarized in figure 5 that the wake flow was entirely steady and the low-speed side was deflected toward the high-speed side as soon as the strength of the suction volume flux exceeded the critical value for the given parameter set. An illustration of this effect is shown in figure 6 where a velocity-vector plot of the steady flow field for $R = 160$, $r = 0.2$ with $\delta_1 = \delta_2 = 1.2$ is exhibited. It is clearly evident that the maximum wake deficit at $x = 3.5$, the last downstream station where the velocity vectors are plotted, is shifted upward toward the high-speed side. The near-wake saddle point of the streamline pattern is also observed to be shifted upward. By comparison, when a similar velocity-vector plot is examined (not shown here) of the time-averaged flow field when U_0 is decreased to a value slightly below $U_{0_{crit}}$ and vortex shedding is active for the same configuration, there is an imperceptible transverse shift in the maximum wake deficit or in the near-wake saddle point from the geometrical centreline of the flow field, even though the mean flow is asymmetric ($r = 0.2$). It is worth noting that the suction distribution was uniform for the simulation shown and, therefore, is not responsible for stimulating any alteration of the symmetry of the flow. The uniform suction entrains a greater volume of fluid from the low-speed stream than from the high-speed stream. The result is a local re-direction of the flow. However,

https://doi.org/10.1017/S0022112096004818 Published online by Cambridge University Press

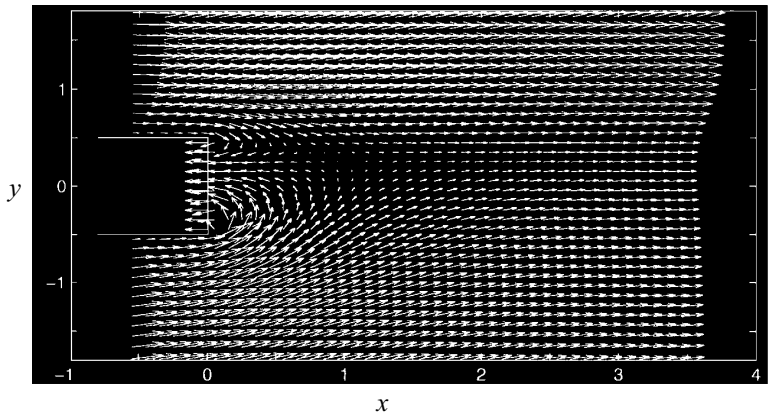


FIGURE 6. The steady velocity field in the near-wake region with supercritical suction distributed uniformly across the entire base ($r = 0.2,\ R = 160,\ q = 0.5$).

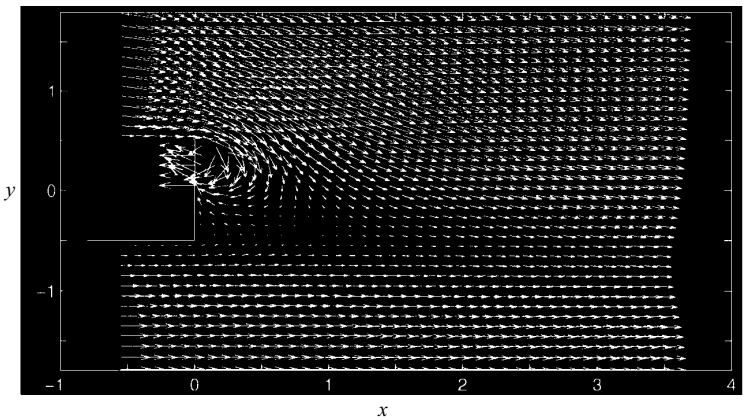


FIGURE 7. The steady velocity field in the near-wake region with supercritical suction distributed uniformly across the half of the base adjacent to the high-speed stream ($r = 0.2,\ R = 160,\ q = 0.5$).

this vectored state can only be achieved after all global modes are suppressed through reduction of the region of absolute instability in the near wake.

With the foregoing results to hand, another simulation was performed with the same flow parameters as in figure 6 and the same supercritical suction volume flux, but the suction was now distributed uniformly over only the (upper) half of the base adjacent to the high-speed side. The response for this asymmetric stimulation is shown in figure 7. One now observes that the suction entrains fluid mostly from the high-speed stream and that the high-speed stream is deflected toward the low-speed side. Consequently, we discover that control of the vectoring *direction* of the near-wake flow can be achieved by selectively varying the *distribution* of the suction volume flux along the base. This vectoring control is possible even in an existing asymmetric flow and with a response in a direction opposite to that selected naturally in the presence of a symmetric stimulation.

The near-wake vectoring described above is accomplished by either exploiting existing asymmetry in the mean flow field or by creating an asymmetry through the control input provided via modified boundary conditions. We emphasize again that the effectiveness of the control input is dependent on the prior suppression of global

https://doi.org/10.1017/S0022112096004818 Published online by Cambridge University Press

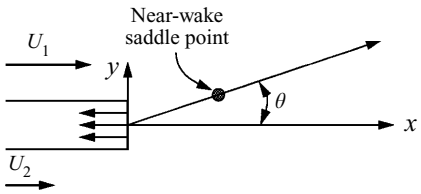


FIGURE 8. Definition of the flow vectoring angle θ.

instabilities in the flow. Now, it has been firmly established that the global dynamics in a wake can be suppressed by the application of either base blowing or suction. The use of base bleed to suppress vortex shedding has been demonstrated by a number of researchers (cf. Wood 1964; Bearman 1967; Hannemann, Lynn & Strykowski 1986; Hannemann & Oertel 1989; and Schumm *et al.* 1994). The results presented here reveal, however, that suction has distinct advantages over blowing when the objective is to vector the near-wake flow field. Base bleed effectively washes out any asymmetry in the near wake and, thereby, dramatically reduces the potential for flow vectoring. On the other hand, base suction accentuates the asymmetries present in the flow, either pre-existing or injected through the control, thereby increasing the potential for flow vectoring. Furthermore, suction can be used to inject additional asymmetries, or overcome existing ones, to obtain selected outcomes.

Quantitative measures of the flow vectoring of the near wake were obtained in two ways: first, by computing the angular displacement of the near-wake saddle points from the wake centreline, specified by the angle θ defined in figure 8; and, second, by computing the normal force per unit span F_N acting on the forebody. The angular displacement θ is evaluated for the time-averaged flow when vortex shedding is active. When vortex shedding is suppressed, the flow is steady and the value of θ is unambiguous. The normal force, assumed to be positive when acting upward (i.e. acting from the low-speed side toward the high-speed side), was evaluated by application of the integral form of the momentum equation using the perimeter of the computation domain as the control surface. Results are presented in terms of the force coefficient

$$C_N = \frac{F_N}{\frac{1}{2}\rho U_\infty^2 b}. \tag{4.1}$$

Another important measure of the flow over the forebody is the base pressure coefficient C_p, which was obtained by evaluating the average of the directly computed pressure distribution along the base of the forebody.

The flow-vectoring angle was computed from a number of simulations performed with different velocity ratios at two different Reynolds numbers when the suction is uniformly distributed across the entire base. Results are exhibited in figure 9. A slight asymmetry, which increases with increasing velocity ratio, is present in the time-averaged flow field at subcritical values of the suction volume flux, especially at the low-Reynolds-number condition. However, as already noted in reference to figure 6, there is a very noticeable vectoring of the low-speed stream upward toward the high-speed stream when the suction flux exceeds the critical value for the suppression of vortex shedding. This is reflected in the increased vectoring angle as the suction flux exceeds the critical value. The onset of flow vectoring is seen to be quite abrupt at the high-Reynolds-number condition. Furthermore, the magnitude of this vectoring increases as the asymmetry of the ambient flow is increased. These curves can be viewed as symmetry-breaking bifurcation diagrams for the flow where the suction

https://doi.org/10.1017/S0022112096004818 Published online by Cambridge University Press

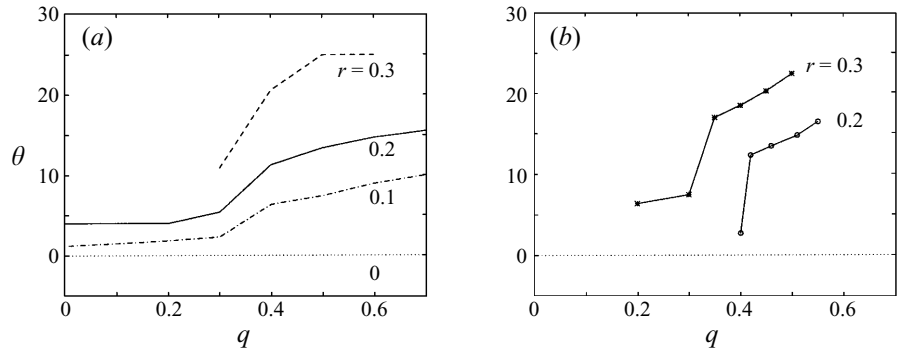


FIGURE 9. The flow vectoring angle as a function of the suction volume flux for suction distributed uniformly across the entire base. (*a*) $R = 160$; (*b*) $R = 520$.

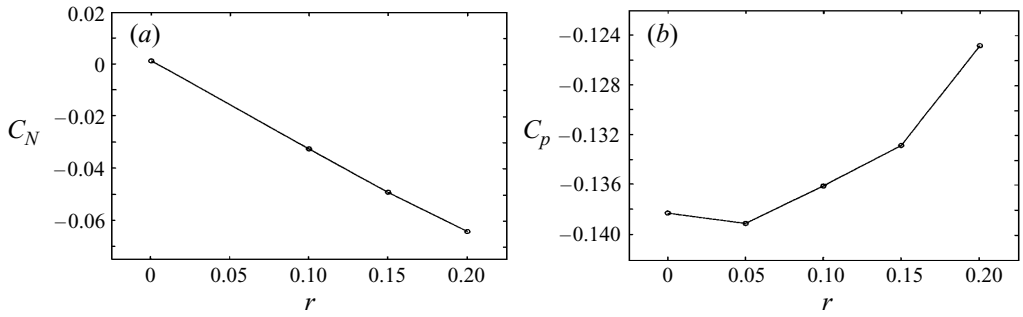


FIGURE 10. The influence of shear on the time-averaged normal force coefficient (*a*) and base pressure coefficient (*b*) in the absence of base suction ($R = 160$).

volume flux serves as the control parameter. Of course, one should recall from figure 5 that the critical value of the control parameter varies for the different conditions (i.e. values of R and r) shown in figure 9.

A more meaningful measure of the vectoring of the flow is obtained by computing the normal force coefficient C_N. In this case it is useful to have some indication of the magnitude of the transverse force acting on the forebody in the presence of an asymmetric flow while vortex shedding is active. The time-averaged values of C_N and C_p were computed for wakes without any suction at $R = 160$, $\delta_1 = \delta_2 = 1.2$ and results are shown in figure 10. One observes that there is a slight negative (downward) force which increases with increasing velocity ratio. This is consistent with the small positive turning angles shown in figure 9 at zero suction. A favourable (for drag purposes) reduction in the base pressure also occurs as the flow asymmetry increases. Although the trend in these results is clear, and the value of C_N at $r = 0$ is indeed close to zero ($C_N(r = 0) = 0.002$), essentially satisfying the symmetry condition, calculations at different conditions were made to define the reliability of reported values of C_N. A worst case value of $C_N = -0.025$ was found for a symmetric wake at $R = 320$. Consequently, reported values of C_N which follow can be accepted with good confidence.

To quantify the potential for vectoring the near wake, two series of simulations were performed for $R = 320$, $\delta_1 = \delta_2 = 1.2$ at a fixed supercritical suction volume flux of $q = 0.5$. In the first series the suction was distributed uniformly over the entire base of the forebody and the near wake was vectored toward the high-speed side. The results

https://doi.org/10.1017/S0022112096004818 Published online by Cambridge University Press

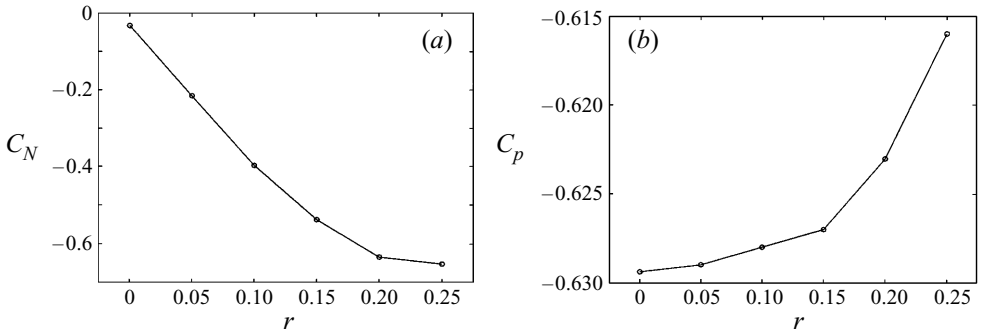


FIGURE 11. The influence of shear on the normal force coefficient (*a*) and base pressure coefficient (*b*) in the steady wake formed with supercritical suction flux with suction distributed uniformly across the base (i.e. vectoring of the low-speed stream toward the high-speed stream). $R = 320,\ q = 0.5,\ \delta_1 = \delta_2 = 1.2$.

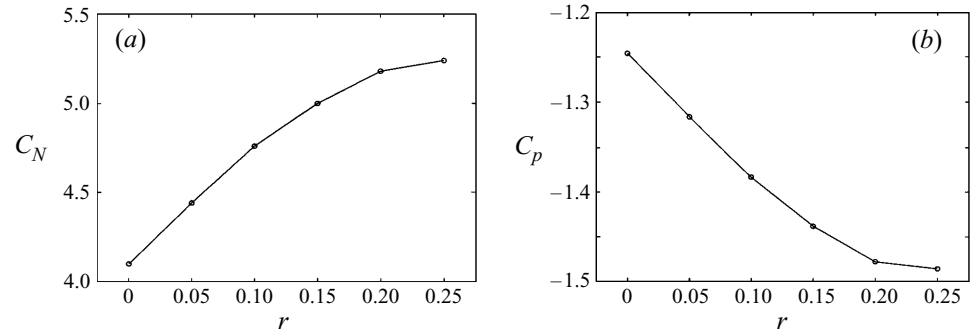


FIGURE 12. As figure 11 but with suction distributed uniformly over only the top half of the base (i.e. vectoring of the high-speed stream toward the low-speed stream). $R = 320,\ q = 0.5,\ \delta_1 = \delta_2 = 1.2$.

for this series are summarized in figure 11. The normal force is an order magnitude larger for the vectored state than it is for the unvectored state shown in figure 10(*a*). The magnitude of the normal force increases monotonically with the velocity ratio with some suggestion that the force may asymptote as the shear increases beyond about $r = 0.3$. The base pressure deficit also decreases in this vectored flow state, but it is still about five times larger than its value in the unvectored state (cf. figure 10*b*.) The suction distribution was confined to the top half of the base, keeping the total volume flux fixed at $q = 0.5$ in the second series of simulations. The results for this series where the high-speed stream is vectored downwards are shown in figure 12. The normal force now acts upward and is an order of magnitude larger than that found in figure 11 for the vectoring of the low-speed stream upward. Of course, the entrainment from the boundary layer on the high-speed side is now much larger than from the boundary layer on the low-speed side because the suction velocities near this side are now twice as large. In both cases, however, it is very evident that the vectored response increases as the inherent asymmetry of the flow increases.

The foregoing results show a decided effect arising from the suction distribution. In fact, they suggest that the suction distribution and volume flux are likely to be important independent parameters in constructing an optimal stimulation to achieve a given vectored state. Of course, practical considerations limit the spectrum of suction distributions that are reasonable. For the purposes of this study, the distributions are

https://doi.org/10.1017/S0022112096004818 Published online by Cambridge University Press

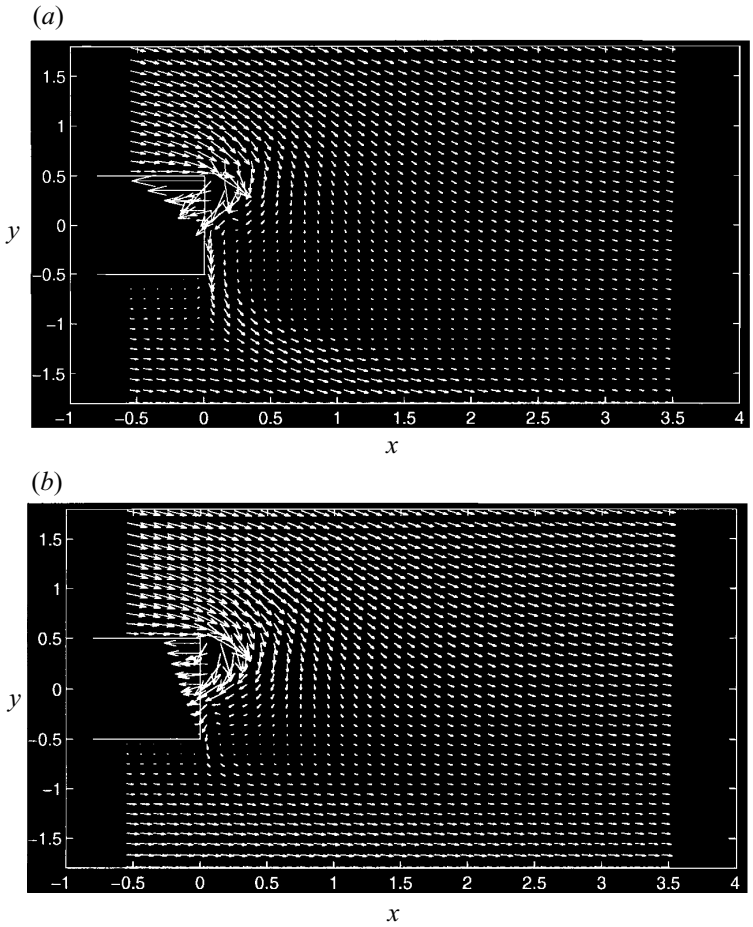


FIGURE 13. The steady velocity field in the near wake of a high-speed vectored flow having a fixed supercritical volume flux arising from different triangular-shaped distributions of suction velocity: (*a*) suction distributed over the top-half of the base; (*b*) suction distributed over the entire base. $R = 320,\ r = 0.2,\ q = 1,\ \delta_1 = \delta_2 = 1.2$.

either uniform, as in the cases already presented, or triangular and extend over either the entire base or are confined to one half of the base adjacent to one of the streams. Two examples involving vectoring of the high-speed stream are shown in figure 13 for a strongly supercritical suction flux of $q = 1.0$. If the suction distribution was uniform across the base, the low-speed stream would be vectored upward. With a triangular distribution skewed toward the high-speed side, the flow is vectored downward toward the low-speed side. If the triangular suction distribution is confined to the top half of the base, a strong downward wall jet is formed along the lower half of the base resulting in a strong vectoring of the high-speed stream. The calculated normal force on the forebody yields $C_N = 7.40$ and $C_N = 6.18$, respectively, for the two flows shown in figures 13(*a*) and 13(*b*). Clearly, the suction distribution can have a very significant role in the vectoring of the near wake.

Further simulations were performed covering a range of supercritical suction fluxes to see if an optimal flux exists for a fixed distribution or if the vectoring response increases monotonically with increased forcing. Since base suction draws fluid princi-

https://doi.org/10.1017/S0022112096004818 Published online by Cambridge University Press

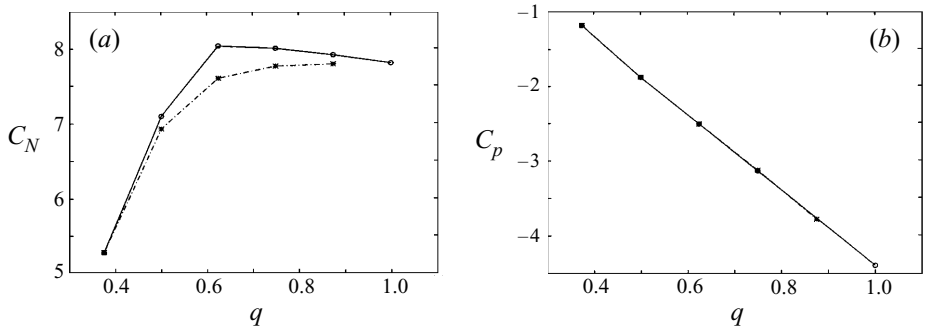


FIGURE 14. The influence of suction volume flux on the normal force coefficient (*a*) and base pressure coefficient (*b*) for a high-speed vectored flow arising from a triangular-shaped suction distribution over the top half of the base. $R = 320$; $r = 0.2$; (——) $\delta_1 = \delta_2 = 1.2$; (— · — · —) $\delta_1 = \delta_2 = 0.9$.

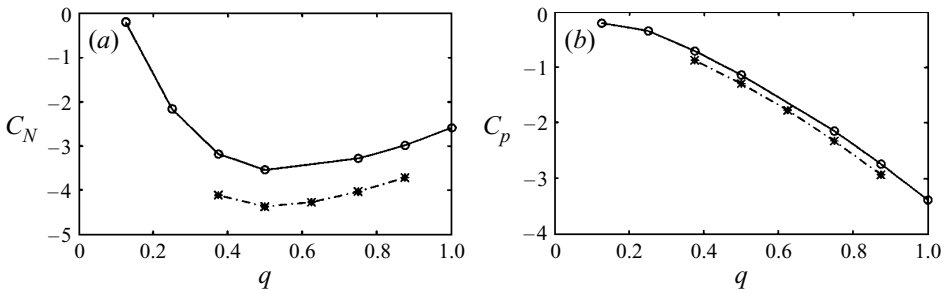


FIGURE 15. As figure 14 but for a low-speed vectored flow arising from a triangular-shaped suction distribution over the lower half of the base.

pally from the boundary layer region, one expects that the boundary layer thickness on the forebody just prior to separation will also have a role in determining the vectoring response. To this end simulations with different inlet boundary layer thicknesses were included in the study. Results for triangular suction distributions over only half the base are shown in figures 14 and 15, respectively, for vectoring the high-speed stream and for vectoring the low-speed stream. In each case, the maximum suction velocity in the distribution is positioned next to the stream to be vectored. Included in the figures are results for two different boundary layer thicknesses. It is apparent that an optimal suction flux exists, at least for the low-speed vectoring shown in figure 15. Examining figure 15 one observes that the optimal flux does not vary significantly with the boundary layer thickness, but the magnitude of the normal force increases as the boundary layer thickness decreases. Interestingly, the high-speed vectoring results in figure 14 show an opposite trend with the boundary layer thickness, although the dependence on the boundary layer thickness is much weaker. One also observes that the base pressure coefficient is essentially independent of the boundary layer thickness for these vectoring results, especially for the case of high-speed-stream vectoring where the differences are indiscernible.

The dependence of such global vectoring quantities as the normal force and the average base pressure on the boundary layer thicknesses was explored further by conducting a set of simulations covering a wider range of δ. For this sequence the suction flux was set at the fixed value $q = 1.0$ which is believed to be significantly removed from the value of q where changes occur because of small departures from the optimal value. Furthermore, a triangular distribution of suction covering the

https://doi.org/10.1017/S0022112096004818 Published online by Cambridge University Press

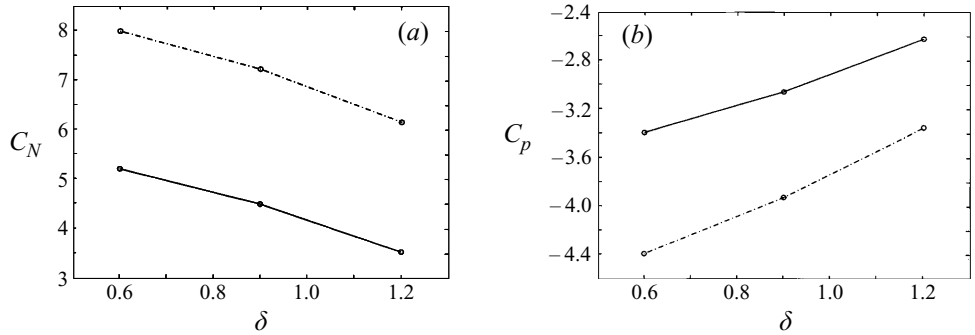


FIGURE 16. Variation of the normal force coefficient (*a*) and base pressure coefficient (*b*) with suction volume flux for a high-speed vectored flow with a triangular-shaped suction distribution extending across the entire base. $R = 320$; $q = 1$; ——, $r = 0$; — · — · — $r = 0.2$.

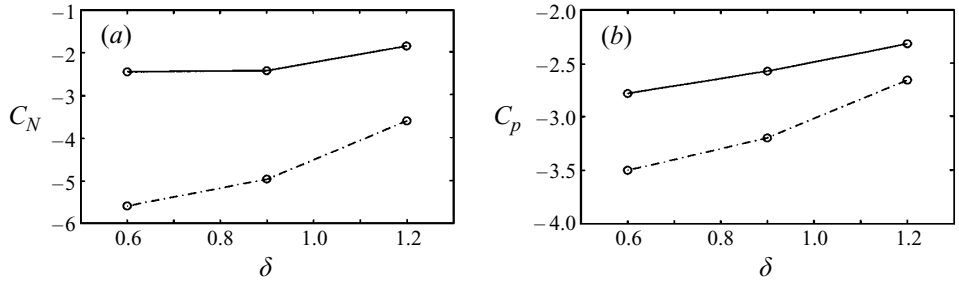


FIGURE 17. As figure 16 but for a low-speed vectored flow with a triangular-shaped suction distribution extending across the entire base.

entire base of the forebody was employed to avoid extremes in the asymmetry of the control effect. With the maximum suction occurring near the top of the base, the results for vectoring the high-speed stream downward shown in figure 16 are obtained. When the triangular distribution is inverted, the vectoring occurs in the opposite direction yielding the results exhibited in figure 17. Results are shown in both figures for a symmetric wake ($r = 0$) and an asymmetric wake with a velocity ratio of $r = 0.2$. Clear trends with δ are found in each case and the opposing variations noted earlier in figures 14 and 15 do not persist. The vectoring response measured in terms of the magnitude of the normal force is now seen to increase, at fixed suction flux and distribution, as the boundary layer thickness decreases. One might argue that the suction volume flux required to achieve a given vectored response (e.g. the normal force) might be related to the displacement effect in the boundary layer of the stream to be vectored. This would imply that the effect of the boundary layer thickness should be evaluated for conditions where the volume flux normalized by the ambient-stream speed and the displacement thickness is held constant. However, this normalization of the suction volume flux cannot account completely for the effect of the boundary layer thickness when an optimal volume flux exists such as shown in figure 15. Consequently, we conclude that there is a decided effect of the boundary layer thickness on the vectoring response arising from a given stimulation which is distinct from its contribution to the specification of the critical suction flux required to suppress vortex shedding (i.e. through the length scale used in the Reynolds number).

The results shown in figures 16 and 17 serve to emphasize a point which has been

https://doi.org/10.1017/S0022112096004818 Published online by Cambridge University Press

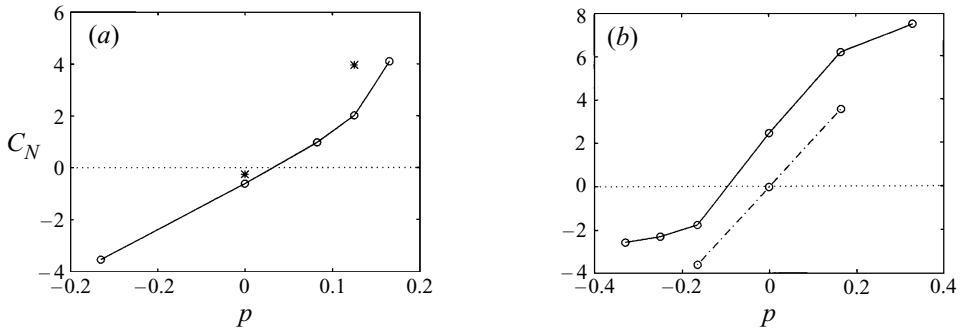


FIGURE 18. Variation of the normal force coefficient with the suction distribution asymmetry parameter p when the suction volume flux exceeds the critical value. (a) The effect of Reynolds number for an asymmetric base flow with $r = 0.2$ and a suction volume flux $q = 0.5$ (—, $R = 160$; $*$, $R = 320$). (b) The effect of velocity ratio in a wake with $R = 520$ and a suction volume flux $q = 1.0$. Data points at $p = \pm 0.17$ coincide with results for simulations using $R = 320$ and $q = 1$.

alluded to previously. It is evident that an asymmetric suction distribution is effective in vectoring an otherwise symmetric flow and that the response is amplified by an existing asymmetry within the essentially parallel flow. If a flow is entirely symmetric, some asymmetry must be injected through the flow control procedure in order to stimulate a vectoring of the flow. If the flow possesses an inherent asymmetry, it can be vectored by an appropriate symmetric stimulation, but the response can be amplified by the injection of further asymmetry through the flow control stimulus. The symmetry of the basic flow and the control are important elements in aerodynamic vectoring. Of course, the effectiveness of any procedure to stimulate an aerodynamic vectoring of a near-wake flow, however, only becomes operative (or, as a minimum, is greatly enhanced) when all global instabilities are suppressed.

In many applications it is desirable to have proportional control. Since the onset of a vectoring response appears quite abruptly as the suction volume flux exceeds the critical value needed to damp out any global instability, proportional control can be realized by varying the suction distribution. That is, one can use symmetry effects to achieve the desired control response. This is illustrated in figure 18 where results are presented for the response of given flows to a varying distribution of suction. The abscissa p in both parts of the figure is the first moment of the suction distribution

$$p = \int_{-1/2}^{1/2} y U_0(y) \mathrm{d}y. \tag{4.2}$$

The results are obtained from a sequence of simulations with a fixed supercritical value of the suction volume flux and using only a linear variation of $U_0(y)$. Positive values of p have the highest suction velocity on the high-speed side and negative values have the strongest suction next to the low-speed side. A clear proportional response can be realized through variation of the control parameter p, holding all other flow parameters (i.e. q, r and R) fixed. Further control of the response can be obtained by simultaneously varying the magnitude of the suction flux q. In figure 18(a) the suction volume flux is $q = 0.5$ and the results are for an asymmetric wake with $r = 0.2$ at two Reynolds numbers. Since the basic flow is also asymmetric, the normal force vanishes for a positive value of p. Figure 18(b) presents results for both symmetric and asymmetric wakes with $q = 1.0$. At this higher value of q the normal force is

https://doi.org/10.1017/S0022112096004818 Published online by Cambridge University Press

shifted upward (to higher values) at fixed asymmetry of the suction distribution. The reversal in response relative to the symmetric suction distribution point $p = 0$ occurs because, as already evident in figures 14 and 15, there exists an optimal volume flux for a given suction distribution. The saturation of the response at higher values of $|p|$ is also believed to arise from the fact that $|C_N|$ is more strongly peaked around the optimal value of q as $|p|$ increases. Clearly, an optimal performance map could be constructed by varying q at fixed p, but the results presented here are sufficient to establish the character of the vectoring response as a function of the key parameters.

5. Summary

A methodology has been found whereby selective control of the flow direction in the near wake behind a bluff body can be realized. The approach is completely devoid of any mechanical motion of physical surfaces or boundaries which define the flow domain and, therefore, can be legitimately termed a technique for *aerodynamic vectoring* of the flow. The input which is used to stimulate and control the vectored response involves distributed suction applied in the base region of the forebody. The volume flux which is removed through the base must, if measurable vectoring of the near wake is to be realized, exceed the well-defined critical value required to suppress any global dynamics manifested by vortex shedding. When a global mode is active in a flow, it endows that flow with a 'structural rigidity' determined by the underlying streamwise eigenfunction. Such a flow is quite resistive to any modification of local boundary conditions, regardless of their symmetry or asymmetry. However, when all global modes are damped, the local flow in the near-wake region can be readily and selectively re-directed. The directional response can be controlled through the spatial distribution of suction velocities along the base and derives from differential entrainment from the boundary layers on either side of the forebody. Wake bleed or blowing from the base can also be used to suppress vortex shedding, but this means of suppression of global dynamics tends to wash-out existing asymmetry possessed by the mean flow. Suction, on the other hand, accentuates any existing asymmetry resident in the mean flow. Furthermore, an asymmetric distribution of suction can be employed in an otherwise symmetric flow to create a radically asymmetric, or vectored, response. The results presented here suggest that an optimal suction flux exists whereby one can achieve a maximal vectoring of the near wake for a given suction distribution and ambient flow state. Also, those distributions of suction velocity which preferentially entrain fluid from the boundary layer on a given side of the base region will be most effective for the vectoring of the stream on that side of the wake.

The suction volume fluxes required to realize suppression of global dynamics and the onset of flow vectoring in the present study appear relatively large when compared to values commonly used in boundary layer control applications. Of course the goals in the respective cases are quite different. In boundary layer control, no global redirection of the flow is intended and no significant changes in the normal force are realized. Applications of the results presented here might include the development of an aerodynamic flap behind an airfoil section having a blunt trailing edge, or the thrust vectoring of a two-dimensional jet in co-flow where the jet lips are blunt-based. In the latter case, the near wakes behind the blunt-based lips at the jet exit would be vectored in concert; that is, a suction distribution leading to a vectoring of the low-speed co-flow stream toward the high-speed jet flow would be applied at one lip and a distribution leading to a vectoring of the high-speed jet stream toward the

https://doi.org/10.1017/S0022112096004818 Published online by Cambridge University Press

lower-speed co-flow stream would be applied on the other side. Some preliminary simulations aimed at exploring these ideas show promise, albeit the Reynolds numbers in studies to date are quite low.

This work was supported by AFOSR under Contract numbers F49620-92-J-0377 and F49620-94-1-0358. Computer resources provided by the San Diego Supercomputer Center were used in obtaining a substantial portion of the results presented here. D. H. acknowledges partial support from a Rockwell International Graduate Fellowship.

REFERENCES

Ashley, S. 1995 Thrust vectoring: a new angle to air superiority. *Mech. Engng* **117**, 58–64.

Bearman, P. W. 1967 The effect of base bleed on the flow behind a two-dimensional model with a blunt trailing edge. *Aero. Q.* **18**, 207–224.

Chomaz, J.-M., Huerre, P. & Redekopp, L. G. 1988 Bifurcations to local and global modes in spatially developing flows. *Phys. Rev. Lett.* **60**, 25–28.

Chomaz, J.-M., Huerre, P. & Redekopp, L. G. 1990 Effect of nonlinearity and forcing on global modes. In *Proc. Conf. on New Trends in Nonlinear Dynamics and Pattern-Forming Phenomena: The Geometry of Nonequilibrium* (ed. P. Coullet & P. Huerre). NATO ASI Series B, vol 237 pp. 259–274. Plenum.

Chomaz, J.-M., Huerre, P. & Redekopp, L. G. 1991 A frequency selection criteria in spatially developing flows. *Stud. Appl. Maths* **84**, 119–144.

Gilbert, B. 1993 Deflection of high speed jet flows using fluidics. *Bull. Am. Phys. Soc.* **38**, 2315.

Hammond, D. A. & Redekopp, L. G. 1996 Global dynamics of symmetric and asymmetric wakes. *J. Fluid Mech.* **331**, 231–260.

Hanneman, K., Lynn, T. B. & Strykowski, P. J. 1986 Experimental investigation of the wake behind a flat plate with and without the influence of base bleed. *Internal Rep.* IB-221-86-A-26. DFVLR, Goettingen.

Hanneman, K. & Oertel, Jr., H. 1989 Numerical simulations of the absolutely and convectively unstable wake. *J. Fluid Mech.* **199**, 55–88.

Ho, C.-M. & Huerre, P. 1984 Perturbed free shear layers. *Ann. Rev Fluid Mech.* **16**, 365–424.

Huerre, P. & Monkewitz, P. A. 1990 Local and global instabilities in spatially developing flows. *Ann. Rev. Fluid Mech.* **22**, 473–537.

Leonard, B. P. 1979 A stable and accurate convective modelling procedure based on quadratic upstream interpolation. *Comput. Meth. Appl. Mech. Engng.* **19**, 59–98.

Leu, T.-S. & Ho, C.-M. 1993 Free shear layer control and its application to fan noise. *AIAA Paper* 93–3242. AIAA Shear Flow Control Conference, Orlando, FL.

Mathis, C., Provansal, M. & Boyer, L. 1984 The Benard-von Karman instability: an experimental study near the threshold. *J. Phys. Lett.* **45**, 483–491.

Monkewitz, P. A. 1988 The absolute and convective nature of instability in two-dimensional wakes at low Reynolds numbers. *Phys. Fluids* **31** No. 5, 999–1005.

Provansal, M., Mathis, C. & Boyer, L. 1987 Benard–von Karman instability: transient and forced regimes. *J. Fluid Mech.* **182**, 1–22.

Schumm, M., Berger, E. & Monkewitz, P. A. 1994 Self-excited oscillations in the wake of two-dimensional bluff bodies and their control. *J. Fluid Mech.* **271**, 17–53.

Smith, B. L. & Glezer, A. 1994 Vectoring of a high aspect ratio rectangular air jet using a zero net mass flux control jet. *Bull. Am. Phys. Soc.* **39**, 1994.

Sreenivasan, K. R., Strykowski, P. J. & Olinger, D. J. 1986 Hopf bifurcation, Landau equation, and vortex shedding behind circular cylinders. *Proc. Forum on Unsteady Flow Separation* (ed. K. N. Ghia). ASME FED, vol. 52, pp. 1–13.

Washington, D. M., Alvi, F. S., Strykowski, P. J. & Krothapalli, A. 1996 Multi-axis fluidic thrust vector control of a supersonic jet using counterflow. *AIAA J.* **34**, 1734–1736.

Wood, C. J. 1964 The effect of base bleed on a periodic wake. *J. R. Aeronaut. Soc.* **68**, 477–482.

https://doi.org/10.1017/S0022112096004818 Published online by Cambridge University Press